FAILURE MECHANISMS IN FIBER-REINFORCED COMPOSITES

I. M. Daniel
IIT Research Institute
Chicago, Illinois 60616

ABSTRACT

Failure mechanisms in fiber composites are a function of many parameters such as constituent properties, lamination geometry, state of stress, etc. They can be viewed at the microscopic level of fiber-matrix interaction, at the single lamina level and at the macroscopic laminate level. The basic failure mechanisms at the microscopic level include tensile, compressive or shear fracture of the matrix, bond failure of the fiber-matrix interface and tensile or compressive (buckling) failure of the fibers. In angle-ply laminates the first failure in the form of cracks parallel to the fibers occurs when the strain limit of the weakest ply (usually at 90-deg. to the load) is exceeded. This first ply failure is usually not catastrophic. The subsequent behavior of the laminate depends on its notch sensitivity and interlaminar shear strength. Failure patterns are highly influenced by free edges where a three-dimensional state of stress exists with high localized interlaminar shear and normal stresses. A variety of failure modes, not always predictable by theory, have been observed around notches in boron/epoxy, glass/epoxy and graphite/epoxy composites using experimental strain analysis techniques. In uniaxially loaded quasi-isotropic laminates with holes, regions of high strain concentration with nonlinear response develop at characteristic locations around 22.5-deg. off the horizontal axis. Failure starts at these off-axis points in the form of local delamination and fiber breakage and propagates across the width of the plate. The effects of lamination geometry, ply stacking sequence, biaxial stress and hole diameter on failure are discussed. In the case of cracks, failure at the top of the crack usually takes the form of a damage zone consisting of ply subcracking along fiber directions, local delamination and fiber breakage. Final failure occurs when this damage zone reaches some critical size. One noteworthy result was that the strength of quasi-isotropic graphite/epoxy laminates is independent of notch geometry and that there is a critical notch size below which the material becomes notch insensitive.

Introduction

A fiber reinforced composite laminate is made up of a number of variously oriented laminae or plies with each ply consisting of a layer of parallel fibers embedded in a matrix. Failure in composite laminates can be viewed from many levels. At the macroscopic level the laminate is viewed as a homogeneous anisotropic material and failure occurs when the average state of stress exceeds some failure criterion for the laminate. At the "mini" level each ply is regarded as a homogeneous anisotropic layer with its own anisotropic failure criteria. The state of stress in each ply can be determined. Failure of one ply affects the stiffness and remaining strength of the laminate but does not necessarily result in total failure. At the microscopic level, it is recognized that the overall behavior of the composite laminate is intimately related to the internal stress distributions and load transfer between the constituent matrix and fibers. The basic failure modes include tensile, compressive or shear fracture of the matrix, bond failure at the fiber matrix interface, and tensile or compressive failure of the fibers. These modes are not isolated or independent but can interact and trigger each other. Failures on the microscopic level within one ply can cause interply failures (delaminations) and result in through the thickness total laminate failure.

Failure mechanisms in fiber composites are a function of the constituent properties, lamination goemetry, structure geometry including geometric discontinuities, state of stress and environmental conditions. In the present paper failure mechanisms under uniaxial and biaxial stresses are discussed at the lamina level (unidirectional composite), for balanced angle-ply laminates and angle-ply laminates with holes and cracks.

Failure Modes in Unidirectional Composite

Longitudinal Tension

The composite in this case is governed by the ultimate strain of the fibers. The most likely initial failure is a fiber break accompanied by some loss of effective fiber length and high interfacial shear stress near the break (Fig. 1).[1] This fiber break can be followed by a number of failure mechanisms in the surrounding matrix, i.e., transverse cracking in the matrix extending up to the adjacent fibers, fiber debonding for some distance from the newly formed ends or conical shear fracture of the matrix.[2] As the load increases, the size of these failure sites remains relatively unchanged but their number increases throughout the composite causing cumulative weakening. Ultimate failure occurs when the number of localized fractures increases to provide a weak path for complete fracture.

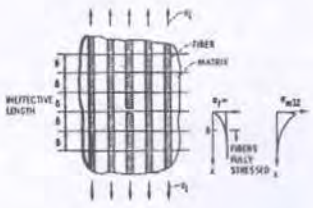

Figure 1. Failure model of unidirectional composite under longitudinal tension (Rosen, 1964).

In the lamina scale three basic failure modes can be distinguished:

(1) brittle
(2) brittle with filament pullout
(3) staggered failure, i.e., brittle failure with filament pullout and matrix shear or debonding along the fibers

These failure modes as discussed by Chamis[3] are illustrated in Fig. 2. Composites with low fiber volume ratio ($v_f \leq 0.4$) exhibit brittle failure, those with intermediate fiber volume ratio ($0.4 \leq v_f \leq 0.65$) exhibit brittle failure with fiber pullout. Plies with high fiber volume ratio ($v_f \geq 0.65$) exhibit the third mode of failure above.

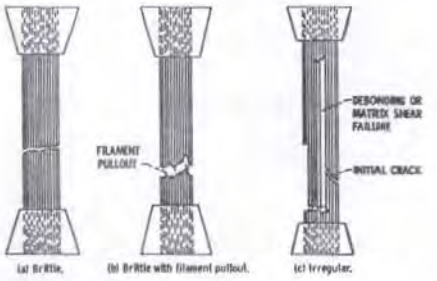

Figure 2. Longitudinal tensile failure model in unidirectional composite (Chamis, 1974).

The longitudinal tensile strength can be predicted reasonably well from the elementary rule-of-mixtures relation

$$S_{11T} + S_f V_f + \sigma_m (1-v_f) \qquad (1)$$

where S_f is the tensile strength of the fibers, and σ_m is the stress in the matrix at a strain equal to the fiber failure strain.

Longitudinal Compression

Compressive behavior of unidirectional composites has been discussed by Greszczuk[4] and Chamis[3]. The characteristic modes of failure in this case are:

(1) Filament microbuckling with matrix elastic and fully bonded.

(2) Matrix yielding or interfacial debonding followed by filament microbuckling.

(3) Panel microbuckling.

(4) Shear failure.

(5) Ply separation by transverse tension.

These failure modes are illustrated in Fig. 3. The first mode of failure occurs in composites with low fiber volume fraction. More realistic composites fail in the second mode above. Shear failure modes have also been observed experimentally. Expressions for the longitudinal compressive strength for microbuckling and interaction modes have been given by Greszczuk.[4]

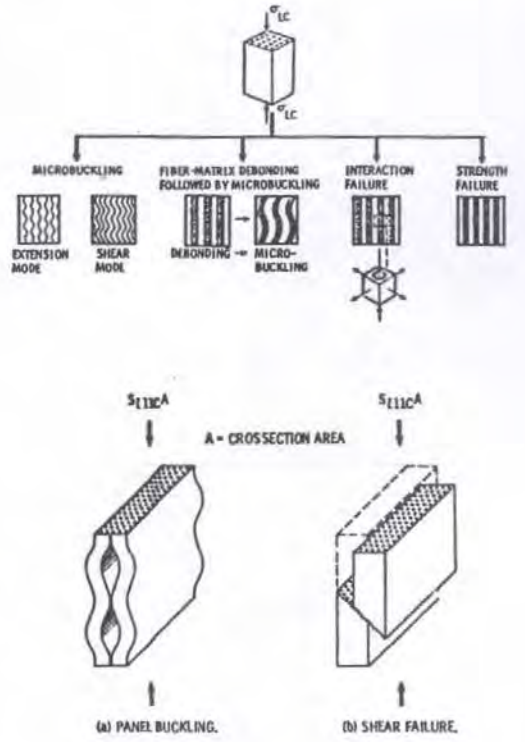

Figure 3. Longitudinal compressive failure modes in unidirectional composite (Greszczuk, 1974; Chamis, 1974).

Transverse Tension

In this case, failure of the composite is dominated by the high strain concentration in the matrix. The primary failure modes are tensile matrix failure and fiber debonding. A great deal of analytical and experimental work has been reported on the stress distributions in transversely loaded unidirectional composites.[5-8] The most significant result is the strain concentration in the matrix at the fiber-matrix interface. An expression for this strain concentration is

$$k_\varepsilon = \frac{\bar{\varepsilon}_y}{\varepsilon_0} = k_\sigma \left(\frac{E_{22}}{E_m}\right) \frac{(1+\nu)(1-2\nu)}{1-\nu} \qquad (2)$$

where

ε_o = average strain

$\bar{\varepsilon}_y$ = maximum strain in the matrix

E_{22} = transverse composite modulus

E_m = matrix modulus

ν = matrix Poisson's ratio

k_σ = stress concentration factor

The stress concentration factor is obtained by analysis or experiment. The variation of the strain concentration factor as a function of fiber spacing is shown in Fig. 4, where it is seen that it rises sharply with increasing fiber volume ratio. Assuming a maximum strain failure criterion for the matrix, a simple expression for the transverse tensile strength is

$$S_{22T} \cong \frac{\varepsilon_{mT}^u}{k_\varepsilon} E_{22} \qquad (3)$$

where ε_{mT}^u is the ultimate tensile strain in the matrix. Greszczuk[4] has given more complex expressions involving three triaxial stress concentration factors.

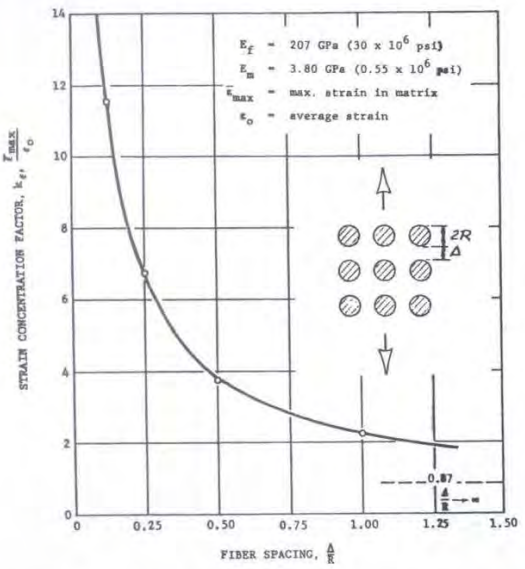

Figure 4. Strain concentration factor as a function of fiber spacing in a square array under transverse loading.

Transverse Compression

The primary failure modes under this type of loading are compressive failure and shear failure in the matrix, sometimes accompanied by fiber debonding. Compressive failure occurs in the matrix when the maximum compressive strain exceeds the ultimate compressive strain. An approximate expression for the strength under this mode of failure can be obtained by replacing ε_{mT}^u with ε_{mC}^u, the ultimate compressive matrix strain, in the compression for tensile strength. A correlation between transverse compressive strength and transverse modulus has been found experimentally.[4]

In-Plane Shear

Failure mechanisms under this loading are matrix shearing, fiber debonding or a combination of the two. The intralaminar shear strength can be determined by dividing the shear strength of the matrix by the shear stress concentrations due to voids and fibers.[4] In many composites the intralaminar shear strength is approximately equal to the interlaminar shear strength. A fairly good correlation has been found between the latter and the transverse tensile strength.[4]

Biaxial Loading

Under biaxial stress conditions one or more of the failure modes discussed before may be activated. Macroscopic and microscopic failure criteria have been proposed.[9,10,11] Macroscopic criteria are based on maximum strain or distortional energy. Heterogeneous microscopic failure criteria taking into consideration nonlinear response have been suggested by McLaughlin and Rosen.[11]

Failure Modes in Angle-Ply Laminates

In angle-ply laminates under uniform stress the first failure in the form of cracks parallel to the fibers of a ply occurs when the strain limit of the weakest ply (usually the one at 90-deg. to the tensile load) is exceeded. Such ply failures are not always detected easily on the macroscopic scale. For example, a change in slope is observed in the axial stress-strain curve of a $[0/90]_s$ graphite/epoxy laminate and a rather sudden change in Poisson's ratio.[12] The strain at the point of slope change equals the failure strain of the 90-deg. ply. The first ply failure is easily predictable and is not always catastrophic. The most challenging problem is the prediction of the subsequent behavior of the laminate following first ply failure.

When a [0/90] laminate, for example, is loaded in uniaxial tension the first cracks appear in the 90-deg. plies. Subsequently, three possible mechanisms of failure propagation can develop (Fig. 5).[12] If the adjacent 0-deg. plies are brittle and notch-sensitive the microcracks will propagate across these plies to cause catastrophic failure (Fig. 5a). This is associated with composites having a low fiber volume ratio and high interlaminar shear strength. If the ply interfaces are relatively weak, i.e., if the material has a low interlaminar shear strength, the cracks in the 90-deg. plies will turn along these interfaces, the initially

cracked ply will be isolated from the other plies and the laminate will continue carrying load with a slightly reduced stiffness and residual strength (Fig. 5b). If the adjacent 0-deg. plies resist crack propagation and if the interlaminar shear strength is high, the initial cracks in the 90-deg. plies do not grow but new similar cracks develop in this ply (Fig. 5c). The 90-deg. ply continues to carry some load through the intact interfaces. Its load carrying capacity is gradually depleted as these cracks become denser and the distance between them shorter.

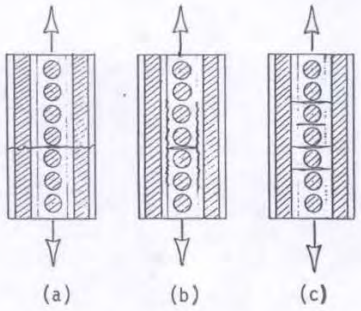

Figure 5. Failure mechanisms in composite laminate following first ply failure: (a) brittle failure, (b) delamination, (c) progressive degradation of 90-deg. ply. (Tsai and Hahn, 1975).

Failure patterns in angle-ply specimens of finite width are highly influenced by the free edges where a three-dimensional state of stress results in highly localized interlaminar shear and normal stresses.[13] Laminates of $[\pm\theta]$ layup under axial loading develop high interlaminar shear stresses which can reach values up to approximately half the normal axial stress. These stresses attenuate very quickly over a distance of approximately one laminate thickness from the edge. For a typical graphite/epoxy laminate they reach the highest value at the edge when $\theta \cong 35$-deg. Such high shear stresses near the free edge often cause progressive edge delamination especially under fatigue loadings. Symmetric angle-ply $[\pm\theta]$ laminates under axial tensile loading in the 0-deg. direction exhibit various failure modes depending on the angle θ. Rotem and Hashin[14] studied these failure modes for glass/epoxy laminates. Stress-strain curves for various values of the ply orientation are shown in Fig. 6. When $\theta < 45$-deg. failure is governed by the high interlaminar shear stress near the edges, which decreases with the angle θ. As the angle θ gets smaller the laminate behavior approaches that of the unidirectional lamina under longitudinal tension. When $\theta = 45$-deg. failure results from progressive lamina cracking over the whole specimen. When $\theta > 45$-deg. lamina cracking occurs early and is more localized resulting in low ultimate strains. As the angle increases the laminate behavior approaches that of the unidirectional lamina under transverse tension.

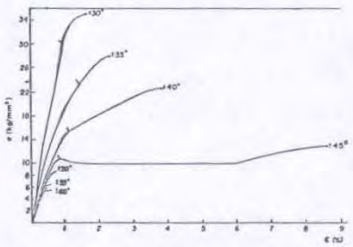

Figure 6. Stress-strain curves of $[\pm\theta]$ angle-ply glass/epoxy laminates (Rotem and Hashin, 1975).

The interaction of failure mechanisms becomes more complex in multi-angle and hybrid laminates having high lamination residual stresses. Residual stresses in laminates are induced during curing as a result of the anisotropic thermal deformations of the variously oriented plies. The influence of residual stresses on failure patterns is vividly illustrated in the case of hybrid angle-ply laminates in Fig. 7. The graphite/glass/epoxy $[\pm 45^C/0^G/0^C]_S$ specimen (where superscripts C and G denote graphite and glass, respectively) failed in a "brooming" fashion after the 0-deg. graphite ply failed first and the isolated layer $(\pm 45^C/0^G)$ curved as shown because of the residual tensile stresses in the 0-deg. glass ply. The same residual stress caused the outer $(0^G/\pm 45^C)$ layer in the $[0^G/\pm 45^C/0^G]_S$ specimens to curl outwards after the central 0-deg. glass plies had delaminated.

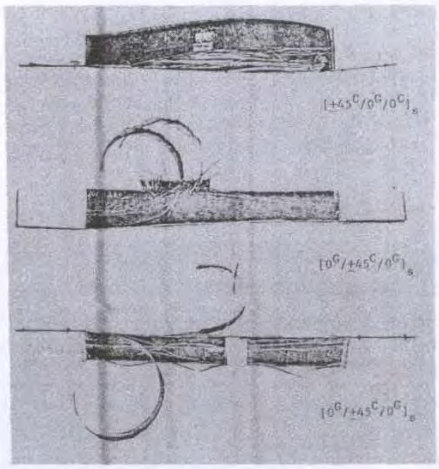

Figure 7. Characteristic failure patterns of three graphite/S-glass/high modulus epoxy specimens under uniaxial tensile loading.

Failure Mechanisms in Laminates with Holes

Of special interest in failure of composites are the failure mechanisms that develop around discontinuities such as holes and cracks, i.e., in the presence of highly nonuniform stress fields. A variety of failure modes, not always predictable by theory, have been observed around notches in boron/epoxy, glass/epoxy and graphite/epoxy composites using experimental strain analysis techniques. The strength and failure modes depend on the type of material, lamination geometry, stacking sequence, hole geometry, hole size, and type of loading.

Uniaxially Loaded $[0/\pm45/0/\overline{90}]_S$ Boron/Epoxy Plate

An experimental strain analysis to failure was conducted for boron/epoxy plates with circular holes using strain gages and photoelastic coatings.[15] Strain distributions in the linear range agree with predictions obtained from linear anisotropic elasticity and finite element analysis. As the load increases a sequence of interacting failure mechanisms consisting of local failure of the 90-deg. ply, local delaminations and finally fiber breakage cause nonlinear strain response, stress and strain redistributions and finally complete failure. The effect of strain redistribution is shown by the strain results of Fig. 8 where the strain near the hole boundary increases nonlinearly at a faster rate and becomes larger than that on the hole boundary. The photoelastic coating fringe patterns of Fig. 9 show that the location of maximum birefringence shifts from θ = 90-deg. (horizontal axis) at low loads to $\theta \cong 67.5°$ deg. near failure. This shift is illustrated by the birefringence variation around the hole boundary for various load levels (Fig. 10). Failure starts at these off-axis points of high birefringence (strain) concentration with nonlinear response. It consists of ply subcracking and local delamination followed by fiber breakage and propagates across the width of the plate to ultimate failure. The failure pattern for this type of specimen is shown in Fig. 11.

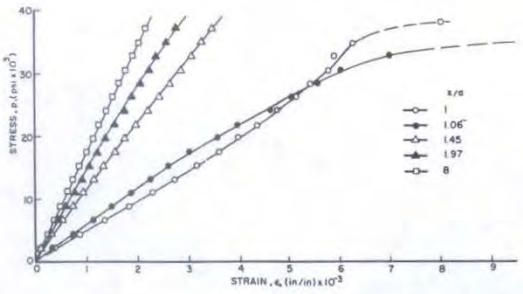

Figure 8. Vertical strains along horizontal axis in $[0/\pm45/0/\overline{90}]_S$ boron/epoxy specimen with 2.54 cm (1 in.) diameter hole under uniaxial tensile loading.

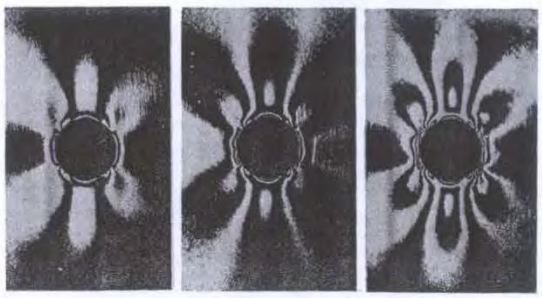

Figure 9. Isochromatic fringe patterns around hole in $[0/\pm45/0/\overline{90}]_S$ boron/epoxy specimen for applied uniaxial stresses of 166 MPa (24.0 ksi), 225 MPa (32.6 ksi) and 293 MPa (42.4 ksi).

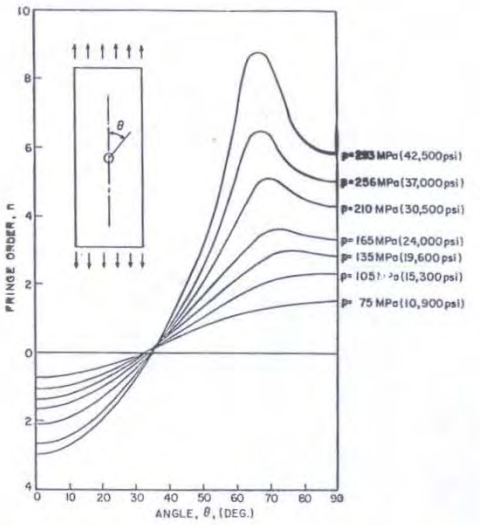

Figure 10. Birefringence distribution around boundary of hole for various load levels in $[0/\pm45/0/\overline{90}]_S$ boron-epoxy specimen.

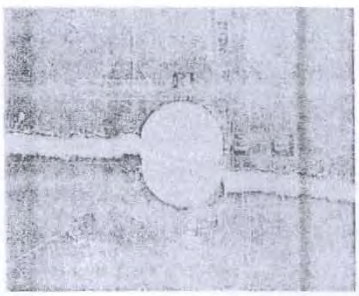

Figure 11. Typical failure pattern around hole in $[0/\pm45/0/\overline{90}]_S$ boron/epoxy specimen under uniaxial tensile loading.

Uniaxially Loaded $[0/\pm45/0/\overline{90}]_S$ Glass/Epoxy Plate

The failure modes in the glass/epoxy plate are similar to those of the boron/epoxy plate above. Failure initiation and propagation are illustrated by the moire fringe patterns of Fig. 12.[16] Cracks start on the hole boundary off the horizontal axis accompanied by extensive delamination. One interesting phenomenon is the seemingly discontinuous propagation of the cracks. They seem to propagate in discrete, discontinuous horizontal steps with a gross direction of fracture at 45-deg. This is possibly due to longitudinal tensile fracture of the outer 0-deg. ply combined with shear delamination of the interior 45-deg. plies. The failure pattern was similar to the one of boron/epoxy but with much more pronounced delamination.

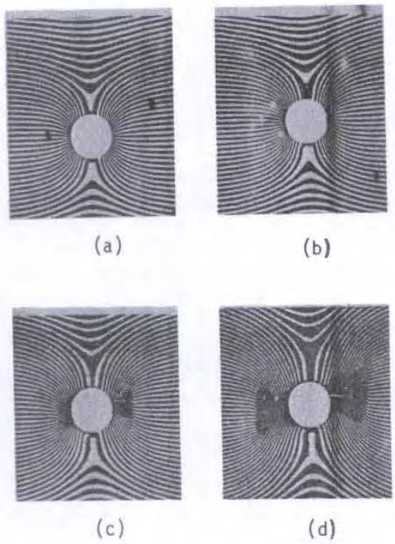

Figure 12. Sequence of moire fringe patterns corresponding to vertical displacements in $[0/\pm45/0/\overline{90}]_S$ glass/epoxy specimen at various applied uniaxial stresses: (a) 198 MPa (28.7 ksi), (b) 206 MPa (29.9 ksi, (c) 206 MPa (29.9 ksi) and (d) 210 MPa (30.4 ksi).

Influence of Laminate Construction

The effect of lamination geometry on failure of plates with holes was studied with boron/epoxy plates of $[0/90/0/90]_S$, $[0_2/\pm45/\overline{0}]_S$, $[0/\pm45/0/\overline{90}]_S$, $[0/\pm45/90]_S$, $[\pm45/0/\pm45]_S$ and $[\pm45/\pm45]_S$ layup.[17] Strain distributions, strain concentration factors, failure modes and strength reduction ratios vary widely with laminate construction. The two extremes of behavior are shown by the fringe patterns for the $[0/90/0/90]_S$ and $[\pm45/\pm45]_S$ plates (Fig. 13). The former shows a sharp strain gradient with a high strain concentration factor (k_ε = 4.82) and with all the perturbation dying out within a short distance from the hole boundary. The maximum birefringence remains at the 90-deg. location. The material behaves in a brittle manner. The first sign of nonlinear response is related to failure of the 90-deg. plies. The maximum strain at failure is low (6.6×10^{-3}). The $[\pm45/\pm45]_S$ plate shows a very moderate strain gradient with a low strain concentration factor (k_ε = 2.06). The influence of the hole extends through the entire width of the plate. The highest fringe concentration occurs on the horizontal axis at or near the hole boundary. The maximum strain at failure is high ($>25 \times 10^{-3}$).

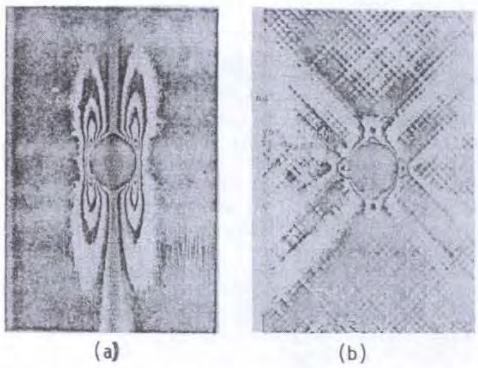

Figure 13. Isochromatic fringe patterns in photoelastic coating around hole in boron/epoxy specimens: (a) $[0/90/0/90]_S$, σ_y = 170 MPa (24.6 ksi), (b) $[\pm45/\pm45]_S$, σ_y = 77 MPa (11.1 ksi).

Failure patterns of the various laminates are shown in Fig. 14. The $[0/90/0/90]_S$ laminate fails in the most brittle fashion through the horizontal axis. The quasi-isotropic laminate $[45/90/0/-45]_S$ failed like the $[0/\pm45/0/\overline{90}]_S$ one discussed earlier, i.e., failure originated on the hole boundary off the horizontal axis, progressed at some angle to the horizontal and finally propagated across the width of the plate in a horizontal direction. Failure in the $[\pm45/0/\pm45]_S$ plate originated off the horizontal axis on the hole boundary and propagated across the width at some angle to the horizontal. The $[\pm45/\pm45]_S$ laminate failed at 45-deg. to the horizontal.

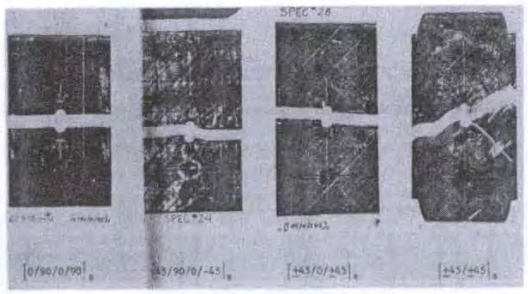

Figure 14. Failure patterns of boron-epoxy panels with holes of various laminate constructions.

The overall laminate strength is related to the number of 0-deg. plies and the strain concentration factor. The strength reduction ratio, i.e., the ratio of the strength of the laminate with a hole to that of a laminate without a hole, was determined for all specimens. In general it is lower for high stress concentration factors. Thus, the $[0/90/0/90]_S$ layup with a stress concentration factor of 4.82 has a strength-reduction ratio of 0.31. At the other extreme, the most flexible layup $[\pm45/\pm45]_S$ with the lowest stress-concentration factor of 2.06 had the lowest strength-reduction ratio of 0.91 which means no strength reduction at all based on the net section. Laminates with a mixture of 0, 45, and 90-deg. plies exhibited stress-concentration factors ranging between 3.08 and 3.34 and strength-reduction ratios between 0.47 and 0.39.

The maximum strain on the hole boundary at failure range in most cases between 8×10^{-3} and 9×10^{-3} in./in., except for the flexible $[\pm45]_C$ construction which withstood strains up to 37×10^{-3} in./in., and the $[0/90]_C$ construction with a maximum strain at failure of 6.6×10^{-3} in./in. In all cases, the maximum strain at failure on the hole boundary was higher than the ultimate tensile-coupon strain.

Influence of Stacking Sequence

Laminates of the same construction but different stacking sequence may have different strengths due to the interlaminar stresses near free edges. The most influencial of these stresses is the interlaminar normal stress. Whenever the free boundary contains a region of high stress concentration (hole) forcing failure initiation in that region, the effects of stacking sequence variation on strength are further accentuated.

Boron/epoxy laminates with holes of $[\pm45/0_2/\overline{0}]_S$, $[0_2/\pm45/\overline{90}]_S$, $[+45/90/0/-45]_S$ and $[45_2/-45_2]_S$ layup were investigated.[17] These represent stacking sequence variations of four of the layups discussed before. The most pronounced differences were observed in the pair of $[0_2/\pm45/\overline{0}]_S$ and $[\pm45/0_2/\overline{0}]_S$ layups. The first one with a measured strain concentration factor of 3.58 was 17 percent stronger than its stacking sequence variation $[\pm45/0_2/\overline{0}]_S$ with a measured strain concentration factor of 4.02. The development of interlaminar normal stresses near the boundary is illustrated in Fig. 15. The first layup with compressive interlaminar normal stress is stronger than the second layup where the interlaminar normal stress is tensile.

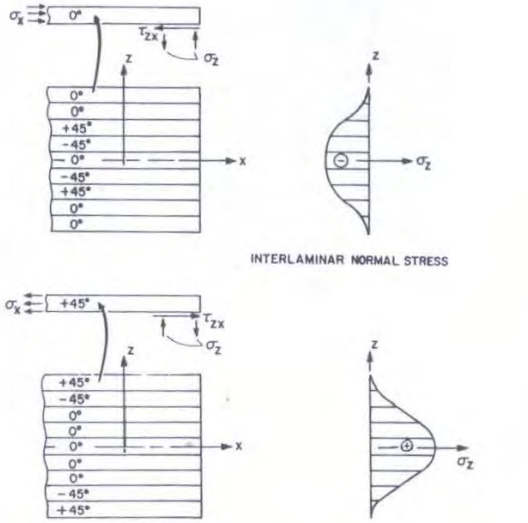

Figure 15. Interlaminar stresses in outer ply and distribution of interlaminar normal stress near the boundary for $[0_2/\pm45/\overline{0}]_S$ and $[\pm45/0_2/\overline{0}]_S$ laminates under uniaxial tensile loading.

Some of the differences between the two layups are also manifested in the isochromatic fringe patterns in the photoelastic coatings (Fig. 16). The pattern for the first layup is fairly symmetrical, has lower birefringence, and shows a tendency for failure propagation along the vertical tangents to the hole boundary, i.e., parallel to the outer 0-deg. plies. The second pattern is antisymmetrical with higher birefringence concentration. The failures in the first and third quadrants are associated with shear failure of the outer ±45-deg. plies, whereas failures in the second and fourth quadrants are associated with cracking along the subsurface 0-deg. plies. The birefringence variation around the circumference of the hole is shown in Fig. 17. The shift of maximum birefringence from θ = 90-deg. to θ = 60-deg. and θ = 65-deg. is shown as well as the higher peak birefringence for the $[\pm45/0_2/\overline{0}]_S$ layup.

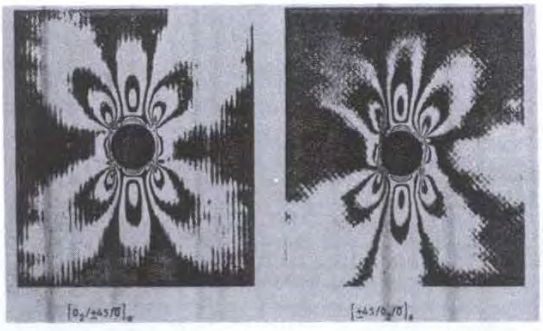

Figure 16. Isochromatic fringe patterns in photoelastic coating around hole in boron/epoxy specimens of two different stacking sequences (σ_y = 392 MPa; 56.8 ksi).

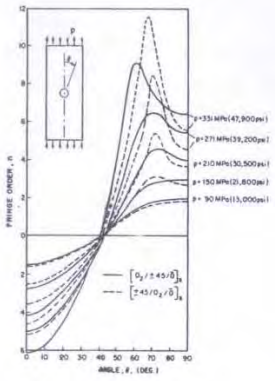

Figure 17. Birefringence distribution around hole boundary at various applied stress levels for two stacking sequence variations.

The stacking sequence variation can affect the failure mode and strength in a dramatic way (Fig. 18). The $[\pm 45/0_2/\overline{0}]_S$ plates tend to fail horizontally through the hole in a catastrophic manner at a relatively low load. The $[0_2/\pm 45/\overline{0}]_S$ plates tend to develop cracking along the vertical tangents to the hole, thus blunting or neutralizing the stress concentration. These specimens subsequently behave like a pair of unnotched laminates and carry a much higher load than the $[\pm 45/0_2/\overline{0}]_S$ specimens.

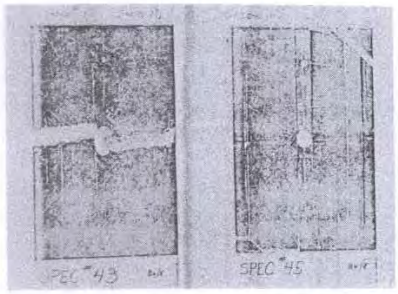

(a) (b)

Figure 18. Failure patterns of boron-epoxy tensile panels with holes: (a) $[\pm 45/0_2/\overline{0}]_S$, (b) $[0_2/\pm 45/\overline{0}]_S$.

Influence of Hole Geometry

The influence of hole geometry was investigated with $[0/\pm 45/0/\overline{90}]_S$ boron/epoxy laminates containing elliptical and square holes.[18] Isochromatic fringe patterns in photoelastic coatings show the characteristic birefringence concentration at points off the horizontal axis for the elliptical holes (Fig. 19). Failure initiates at these points as in the case of the circular hole (Fig. 20). The plates with elliptical holes having the major axis in the vertical and horizontal directions, are only 25 percent stronger and 20 percent weaker, respectively, than plates with an equivalent circular hole. Laminates with a 2.54 cm (1 in.) square hole were slightly stronger than those with a 2.54 cm (1 in.) diameter circular hole.

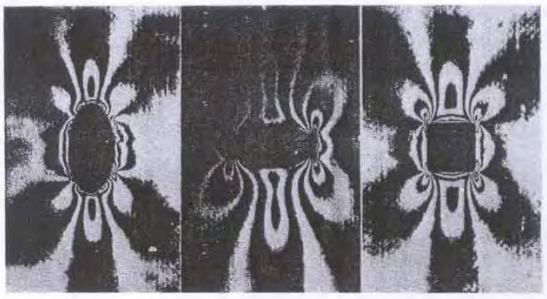

(a) (b) (c)

Figure 19. Isochromatic fringe patterns in photoelastic coating of $[0/\pm 45/0/\overline{90}]_S$ boron/epoxy laminates with elliptical and square holes under uniaxial tensile loading. (a) σ_y = 361 MPa (52.3 ksi), (b) σ_y = 241 MPa (34.9 ksi), (c) σ_y = 331 MPa (48.0 ksi).

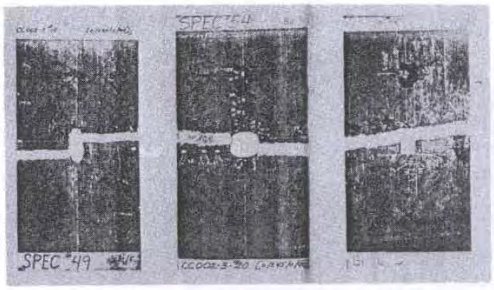

Figure 20. Failure patterns of $[0/\pm 45/0/\overline{90}]_S$ boron-epoxy laminates having elliptical and square cutouts.

Influence of Hole Diameter

Graphite/epoxy plates of $[0/\pm 45/90]_S$ layup with circular holes ranging in diameter between 0.02 cm (0.008 in.) and 2.54 cm (1 in.) were tested under uniaxial tension.[19] The response was similar to that of the quasi-isotropic boron/epoxy specimens discussed before. Strains at and near the hole boundary become nonlinear at a strain corresponding to initial failure of the 90-deg. plies. Maximum measured strains on the hole boundary can reach values up to twice the ultimate strain of the unnotched laminate. Regions of high

strain concentration with nonlinear response develop at four characterisitic locations 22.5-deg. off the horizontal axis. Failure initiates at these points where the interlaminar and membrane shear stresses reach maximum values. The laminate strength decreases with increasing hole size. There is a critical hole size below which the laminate becomes notch insensitive. The strength reduction ratio is plotted as a function of hole radius in Fig. 21. The effect of hole diameter on strength can be satisfactorily explained using the average stress criterion.[20] According to this criterion total failure occurs when the axial stress averaged over a characteristic distance (approximately 4mm) from the hole boundary equals the strength of the unnotched laminate.

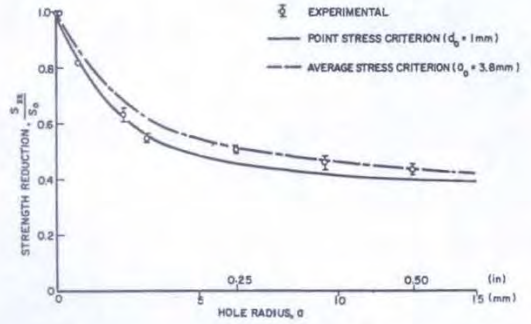

Figure 21. Strength reduction as a function of hole radius for $[0/\pm45/90]_S$ graphite/epoxy plates with circular holes under uniaxial tensile loading.

The effect of hole diameter was also studied with $[0_2/\pm45]_S$ graphite/epoxy plates with holes ranging in diameter between 0.04 cm (0.016 in.) and 2.54 cm (1 in.).[21] Typical strain variation along the horizontal axis are illustrated in Fig. 22 where two levels of nonlinear response are evident. The first one corresponds to a stress redistribution following the nonlinear response of the material under compressive stress at the 0-deg. location. The second level of pronounced nonlinearity occurs as a result of stress and strain redistribution produced by localized compressive failure (delamination) around the 0-deg. location. Failure patterns for specimens with holes of various diameters are shown in Fig. 23. Two failure modes can be discerned. In the case of larger holes failure initiates at locations of the hole boundary approximately 72-deg. from the load axis. In the case of smaller holes the outer 0-deg. plies through the hole tend to separate and, thus, reduce or eliminate the effects of stress concentration. There is a critical hole diameter (approximately 1.6 mm) below which the laminate becomes notch-insensitive. The strength reduction ratio is plotted as a function of hole radius in Fig. 24. The effect of hole diameter can be satisfactorily described using the average stress criterion.

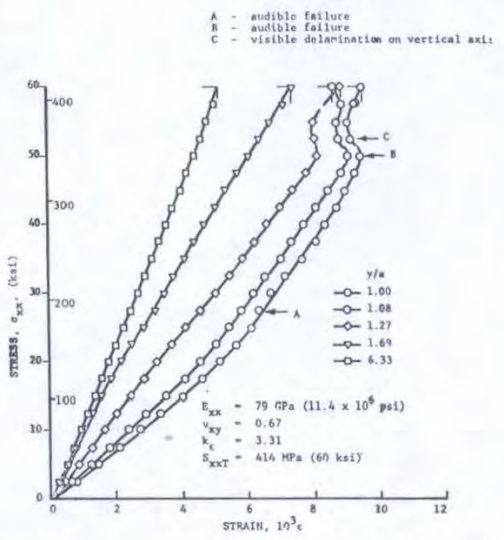

Figure 22. Vertical strains along horizontal axis of $[0_2/\pm45]_S$. Graphite/epoxy specimen with 1.91 cm (0.75 in.) diameter hole under uniaxial tensile loading.

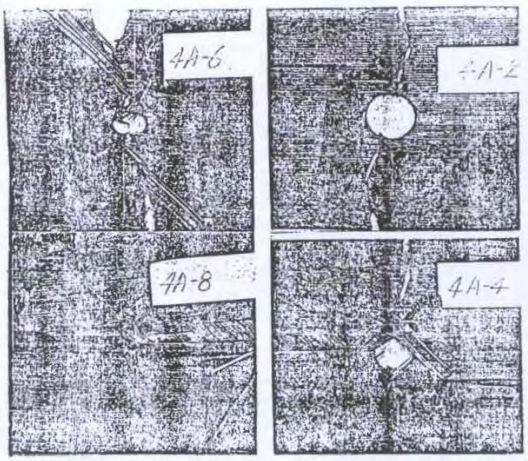

Figure 23. Failure patterns in $[0_2/\pm45]_S$ graphite/epoxy specimens with holes of various sizes under uniaxial tension. (Hole diameters are 2.54 cm (1 in.), 1.91 cm (0.75 in.), 1.27 cm (0.50 in.) and 0.64 cm (0.25 in.).

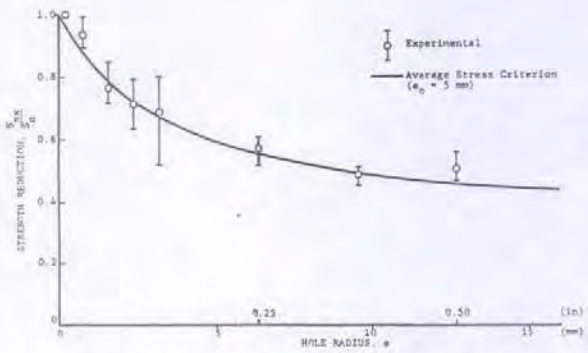

Figure 24. Strength reduction as a function of hole radius for $[0_2/\pm45]_S$ graphite/epoxy plates with circular holes under uniaxial tensile loading.

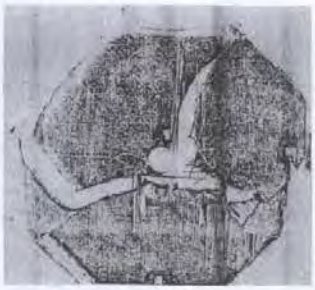

Figure 26. Failure pattern in $[0/\pm45/90]_S$ graphite/epoxy specimen with 1.91 cm (0.75 in.) diameter hole under equal biaxial tensile loading.

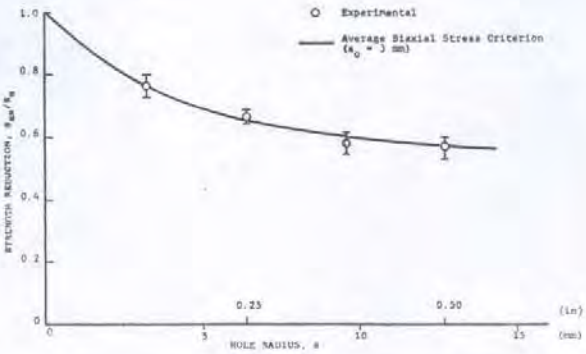

Figure 27. Strength reduction as a function of hole radius for $[0/\pm45/90]_S$ graphite/epoxy plates with circular holes under 1:1 biaxial tensile loading.

Effect of Biaxial Stress and Hole Diameter

These effects were studied by testing $[0/\pm45/90]_S$ graphite/epoxy laminates with holes of diameters ranging between 0.64 cm (0.25 in.) and 2.54 cm (1 in.) under equibiaxial tension.[19] As in the case of uniaxial loading, regions of high strain concentration with nonlinear response develop at eight chracteristic locations approximately 22.5-deg. off the fiber axes as illustrated by the isochromatic fringe patterns of Fig. 25. Failure initiates at one or more of these points. A typical failure pattern is shown in Fig. 26 with cracking and delamination initiated at three locations on the hole boundary. The variation of strength reduction ratio with hole radius was satisfactorily described by using an average biaxial stress criterion (Fig. 27).

Figure 25. Isochromatic fringe patterns in photoelastic coating of $[0/\pm45/90]_S$ graphite/epoxy specimen with 2.54 cm (1-in.) diameter hole under equal biaxial tensile loading (far-field biaxial stress marked).

Failure Mechanisms in Laminates with Cracks

Uniaxially Loaded $[0/90/0/\overline{90}]_S$ Glass/Epoxy Plate

The failure mechanisms around notches in a crossply glass/epoxy laminate are elucidated by the moire fringe patterns of Fig. 28.[22] A high vertical tensile strain-concentration factor, approximately 5, exists at the tip of the crack. This peak strain remains nearly constant for some distance along a vertical line normal to the axis of the crack. This line represents a boundary between high tensile strain in front of the crack and high shear strain behind the tip of the crack. The high in-plane shear stress near the crack tip causes splitting of the 0-deg. plies along the fiber direction, thus producing the discontinuity in the fringe pattern. This failure is accompanied by delamination and horizontal tensile failure with crack propagation along the subsurface 90-deg. plies. The delaminated and sheared outer 0-deg. ply behaves like a bundle of independent fibers; hence, it is under nearly uniform strain in the segment-shaped region it occupies. The affected zone consists of a square region around the hole expanding into circular segments ahead of the crack. As the load is increased the original

vertical shear crack grows in length and new ones appear ahead of the crack.

(a) (b) (c)

Figure 28. Moire fringe patterns around crack in glass-epoxy composites $[0/90/0/\overline{90}]_S$ at three levels of applied stress, (a) σ_y = 76 MPa (11.0 ksi), (b) σ_y = 102 MPa (14.8 ksi), (c) σ_y = 128 MPa (18.5 ksi).

Uniaxially Loaded $[0/\pm45/90]_S$ Graphite/Epoxy Plate - Effect of Crack Length

The deformation and failure of graphite/epoxy plates with cracks of different lengths were investigated with experimental techniques.[19,23] Crack lengths between 0.64 cm (0.25 in.) and 2.54 cm (1 in.) were investigated. Measured strains near the crack tip show two points of rate change at levels of 0.002 and 0.006. The latter corresponds to failure of the 90-deg. plies. Failure at the tip of the crack takes the form of a damage zone consisting of ply subcracking along fiber directions, local delaminations and fiber breakage. The growth of this damage zone is illustrated by the isochromatic fringe patterns of Fig. 29. The damage zone was measured and correlated with the stress intensity factor ($K_I = \sigma\sqrt{\pi a}$) as was done by Mandell et al.[24] Results of this correlation are shown in Fig. 30. The damage zone increases linearly with the square of the stress intensity factor K_I^2 up to a certain value of K_I, which is nearly constant with crack length. Thereafter, this zone increases linearly at a faster rate, which is independent of crack length. Final failure occurs when the damage zone reaches some critical size. The effect of crack length on strength was satisfactorily described using the average stress criterion (Fig. 31). By comparing these results with those obtained from similar specimens with holes (Fig. 27) it was found that strength was independent of notch geometry, i.e., specimens with cracks and holes of the same size had the same strength (Fig. 32).

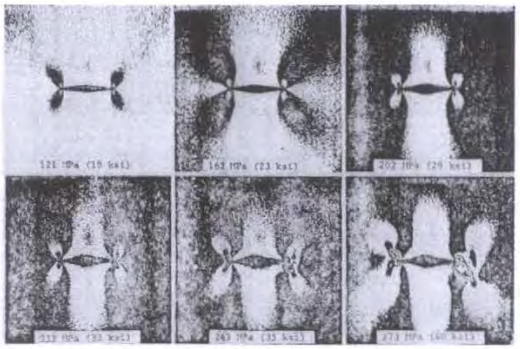

Figure 29. Isochromatic fringe patterns in photoelastic coating around 1.27 cm (0.50 in.) crack of $[0/\pm45/90]_S$ graphite/epoxy specimen at various levels of applied stress.

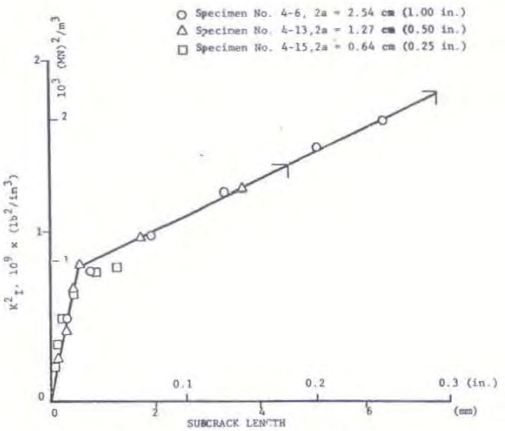

Figure 30. Variation of length of subcrack with square of stress intensity factor for uniaxially loaded $[0/\pm45/90]_S$ graphite/epoxy plates with cracks.

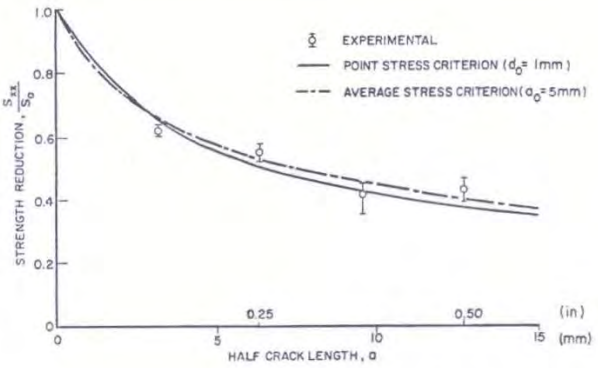

Figure 31. Strength reduction as a function of crack length for $[0/\pm45/90]_S$ graphite/epoxy plates with horizontal cracks under uniaxial tensile loading.

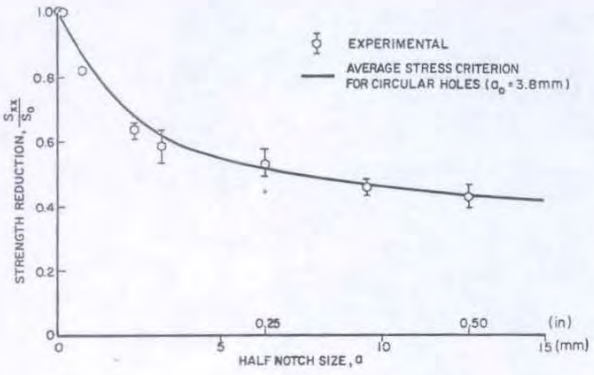

Figure 32. Strength reduction as a function of notch size for $[0/\pm45/90]_S$ graphite/epoxy plates with circular holes and cracks under uniaxial tensile loading.

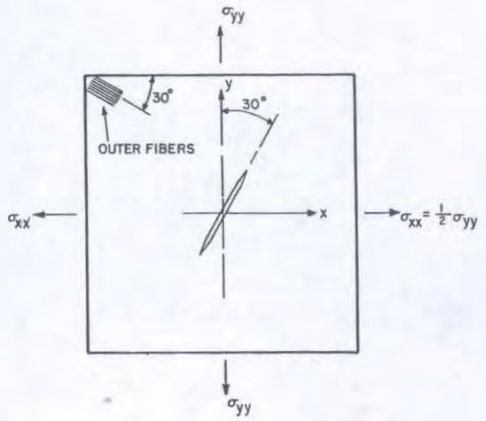

Figure 33. Biaxial loading of $[0/\pm45/90]_S$ graphite/epoxy specimens with cracks.

Effect of Biaxial Stress

Failure mechanisms in biaxially loaded $[0/\pm45/90]_S$ graphite/epoxy plates with cracks were investigated for various crack lengths.[19] Plates with inclined cracks were loaded under 2:1 biaxial tension producing a substantial shear stress along the crack in addition to the crack opening stress. (Fig. 33.) The crack direction was perpendicular to the outer fibers. The shear stress contributes appreciably to the development of the damage zone. The initial crack extension seems to be at 45-deg. to the original crack direction. Thereafter, the damage zone consisting of subcracks parallel to the fibers of the various plies, delaminations and sometimes fiber breakage along the subcracks of the adjacent plies, propagates normally to the crack direction in most cases. Some failure modes are illustrated by the isochromatic fringe patterns of Fig. 34. The size of the damage zone is limited up to a stress of 260MPa (37.7 ksi), then an abrupt jump takes place before the stress level of 278 MPa (40.3 ksi). In addition to the primary damage extension normal to the initial crack, there is secondary crack extension along the original crack direction probably along the fibers of the central plies of the laminate. At the tips of these subsurface cracks tertiary cracks appear normal to the original crack direction as seen in the fringe patterns. A typical failure pattern of a biaxially loaded plate with an inclined crack is shown in Fig. 35.

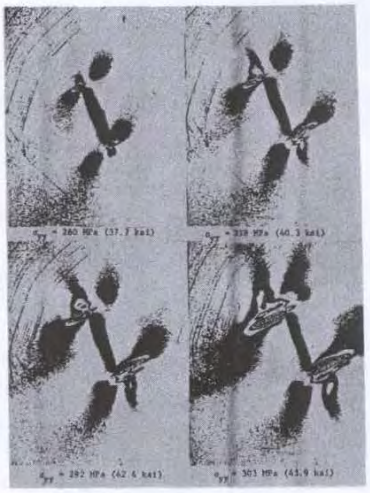

Figure 34. Isochromatic fringe patterns in photoelastic coating around 1.27 cm (0.5 in.) crack in $[0/\pm45/90]_S$ graphite/epoxy specimen under biaxial loading $\sigma_{yy} = 2.03\sigma_{xx}$ at 30-deg. with crack direction.

Figure 35. Biaxial specimen with 1.91 cm (0.75 in.) long crack after failure.

Conclusion

Failure mechanisms in fiber reinforced composites were discussed from the micro-, mini- and macroscopic points of view. All failure mechanisms in composite laminates can be explained in terms of fundamental modes such as tensile, compressive or shear fracture of the matrix, failure of the fiber-matrix interface and tensile or compressive (buckling) failure of the fibers. Failure of the first (weakest) ply in an angle-ply laminate can be predicted theoretically and ascertained experimentally. Subsequent behavior of the laminate following first ply failure is of greater interest and is more difficult to predict. The presence of notches produces a combination of interacting failure mechanisms which are best studied experimentally. Basically, the initial damage zone around notches consists of ply subcracking along fiber directions, delaminations and fiber breakage in adjacent fibers along the initial subcracks. Unlike homogeneous brittle materials, composite laminates tend to be notch insensitive. Cases were discussed where the strength was independent of notch geometry and where a threshold notch size exists below which the laminate becomes notch insensitive.

In structural applications of composites it is important to be able to ascertain the presence, nature and extent of damage by nondestructive techniques. Knowledge of the physical failure mechanisms will enable one to select or develop one or more nondestructive techniques. Knowledge of the physical failure mechanisms will enable one to select or develop one or more nondestructive techniques for better correlation of physical damage and NDE data. Failure criteria, empirical or theoretical, can be used to correlate extent of damage with residual strength of a component. Thus, NDE has the potential of directly determining the residual strength and remaining useful life of a composite structure.

References

1. B. W. Rosen, N. F. Dow and Z. Hashin, "Mechanical Properties of Fibrous Composites," NASA CR-31, April 1964.

2. J. Mullin, J. M. Berry and A. Gatti, "Some Fundamental Fracture Mechanisms Applicable to Advanced Filament Reinforced Composites," J. of Composite Materials, Vol. 2, January 1968, pp. 82-103

3. C. C. Chamis, "Micromechanics Strength Theories," in "Fracture and Fatigue" Vol. 5, (ed. by L. J. Broutman), Composite Materials (ed. by L. J. Broutman and R. H. Krock), Academic Press, New York, 1974.

4. L. B. Greszczuk, "Consideration of Failure Modes in the Design of Composite Structures," AGARD-CP-163, Specialists Meeting on "Failure Modes of Composite Materials with Organic Matrices and Their Consequences on Design," 1975, Section 12.

5. R. L. Foy, "Structural Composites," North American Aviation, Columbus Division, Contract No. AF33(615)-5150, Quart. Reports, No. 1, 2, 3, Sept. 1966, December 1966, March 1967.

6. D. F. Adams and D. R. Doner, "Transverse Normal Loading of a Unidirectional Composite," J. Composite Materials, Vol. 1, 1967, pp. 152-164.

7. I. M. Daniel, "Micromechanics" in "Structural Airframe Application of Advanced Composite Materials," AFML-TR-69-101, Vol. II, September 1969.

8. R. H. Marloff and I. M. Daniel, "Three-Dimensional Photoelastic Analysis of a Fiber-Reinforced Composite Model," Exp. Mechanics, Vol. 9, April 1969, pp. 156-162.

9. S. W. Tsai, "Strength Characteristics of Composite Materials," NASA-CR-224, April 1965.

10. S. W. Tsai and E. M. Wu, "A General Theory of Strength for Anisotropic Materials," J. Composite Materials, Vol. 5, 1971, pp. 58-80.

11. P. V. McLaughlin and B. W. Rosen, "Combined Stress Effects Upon Failure of Fiber Composites," Materials Sciences Corp., Final Report to Naval Air Development Center, TRF/7404/1112, April 1974.

12. S. W. Tsai and H. T. Hahn, "Failure Analysis of Composite Materials," ASME Symposium on Inelastic Behavior of Composite Materials, Houston, Texas, 1975, AMD-Vol. 13, pp. 73-96.

13. R. B. Pipes and N. J. Pagano, "Interlaminar Stresses in Composite Laminates Under Uniform Axial Extension," J. Composite Materials, Vol. 4, October 1970, pp. 538-548

14. A. Rotem and Z. Hashin, "Failure Modes of Angle Ply Laminates," J. Composite Materials, Vol. 9, April 1975, pp. 191-206.

15. I. M. Daniel, R. E. Rowlands and J. B. Whiteside, "Deformation and Failure of Boron/Epoxy plate with Circular Hole," Analysis of the Test Methods for High Modulus Fibers and Composites, ASTM STP 521, American Society for Testing and Materials, 1973, pp. 143-164.

16. R. E. Rowlands, I. M. Daniel and J. B. Whiteside, "Stress and Failure Analysis of a Glass-Epoxy Plate with a Hole," Experimental Mechanics, Vol. 13, January 1973, pp. 31-37.

17. I. M. Daniel, R. E. Rowlands and J. B. Whiteside, "Effects of Material and Stacking Sequence on Behavior of Composite Plates with Holes," Experimental Mechanics, Vol. 14, January 1974, pp. 1-9.

18. R. E. Rowlands, I. M. Daniel and J. B. Whiteside, "Geometric and Loading Effects on Strength of Composite Plates with Cutouts," Composite Materials: Testing and Design (Third Conference), ASTM STP 546, American Society for Testing and Materials, 1974, pp. 361-375.

19. I. M. Daniel, "Biaxial Testing of Graphite/Epoxy Composites Containing Stress Concentrations" - Part I, AFML-TR-76-244, December 1976.

20. J. M. Whitney and R. J. Nuismer, "Stress Fracture Criteria for Laminated Composites Containing Stress Concentrations," J. Composite Materials, Vol. 8, July 1974, pp. 253-265

21. I. M. Daniel, "Biaxial Testing of Graphite/Epoxy Composites Containing Stress Concentrations," Part II, AFML-TR-76-244 June 1977.

22. I. M. Daniel, R. E. Rowlands and D. Post, "Strain Analysis of Composites by Moiré Methods," Experimental Mechanics, Vol. 13, June 1973, pp. 246-252.

23. I. M. Daniel, "Strain and Failure Analysis of Graphite/Epoxy Plates with Cracks," presented at SESA Spring Meeting, Dallas, Texas, May 15-20, 1977.

24. J. F. Mandell, Su-Su Wang and F. J. McGarry, "The Extension of Crack Tip Damage Zones in Fiber Reinforced Plastic Laminates," J. Composite Materials, Vol. 9, July 1975, pp. 266-287.